Rational Design of Graphene-Supported Single Atom Catalysts for Hydrogen Evolution Reaction

*Md Delowar Hossain, Zhenjing Liu, Minghao Zhuang, Xingxu Yan, Gui-Liang Xu, Chaitanya Avinash Gadre, Abhishek Tyagi, Irfan Haider Abidi, Cheng-Jun Sun, Hoilun Wong, Alexander Guda, Yufeng Hao, Xiaoqing Pan, Khalil Amine, and Zhengtang Luo**

The proper choice of nonprecious transition metals as single atom catalysts (SACs) remains unclear for designing highly efficient electrocatalysts for hydrogen evolution reaction (HER). Herein, reported is an activity correlation with catalysts, electronic structure, in order to clarify the origin of reactivity for a series of transition metals supported on nitrogen-doped graphene as SACs for HER by a combination of density functional theory calculations and electrochemical measurements. Only few of the transition metals (e.g., Co, Cr, Fe, Rh, and V) as SACs show good catalytic activity toward HER as their Gibbs free energies are varied between the range of –0.20 to 0.30 eV but among which Co-SAC exhibits the highest electrochemical activity at 0.13 eV. Electronic structure studies show that the energy states of active valence d_{z^2} orbitals and their resulting antibonding state determine the catalytic activity for HER. The fact that the antibonding state orbital is neither completely empty nor fully filled in the case of Co-SAC is the main reason for its ideal hydrogen adsorption energy. Moreover, the electrochemical measurement shows that Co-SAC exhibits a superior hydrogen evolution activity over Ni-SAC and W-SAC, confirming the theoretical calculation. This systematic study gives a fundamental understanding about the design of highly efficient SACs for HER.

1. Introduction

Global warming is one of the most important problems the world currently faces and is increasing rapidly due to extensive use of fossil fuels as the primary source for energy production. On the other hand, the limited fossil fuel reserves coupled with sustainable development vision call for the development of new green technologies for energy production.[1] Hydrogen, an abundant, renewable, and highly dense energy source, has been considered as a potential alternative sustainable energy source.[2] The ideal way to produce hydrogen of high purity and in large quantities is by the electrolytic reduction of water via hydrogen evolution reaction (HER). Naturally, HER has a high energy barrier (known as overpotential, η, the minimum potential required to produce hydrogen above its thermodynamic value), which demands effective catalysts to overcome. Amongst all HER catalysts, platinum is the most efficient to date with a small overpotential in acidic solutions. However, the high cost and scarcity of platinum limit its application for industrial production of hydrogen.[3] Thus, the proper choice of an active, efficient, and durable electrocatalyst from earth's abundant sources remains a major challenge in energy research. In recent years, tremendous effort has been devoted to the invention of new types of heterogeneous electrocatalysts, based on a variety of nonprecious transition metals, including Co, Ni, Mo, Fe, and their derivatives (i.e., nitrides,

---

M. D. Hossain, Z. Liu, Dr. M. Zhuang, Dr. A. Tyagi, Dr. I. H. Abidi, H. Wong, Prof. Z. Luo
Department of Chemical and Biological Engineering
William Mong Institute of Nano Science and Technology, and Hong Kong Branch of Chinese National Engineering Research Center for Tissue Restoration and Reconstruction
The Hong Kong University of Science and Technology
Clear Water Bay, Kowloon 999077, Hong Kong
E-mail: keztluo@ust.hk

Dr. X. Yan, Prof. X. Pan
Department of Materials Science and Engineering
University of California–Irvine
Irvine, CA 92697, USA

The ORCID identification number(s) for the author(s) of this article can be found under https://doi.org/10.1002/aenm.201803689.

DOI: 10.1002/aenm.201803689

Dr. G.-L. Xu, Prof. K. Amine
Chemical Sciences and Engineering Division
Argonne National Laboratory
9700 South Cass Avenue, Lemont, IL 60439, USA

C. A. Gadre, Prof. X. Pan
Department of Physics and Astronomy
University of California–Irvine
Irvine, CA 92697, USA

Dr. C.-J. Sun
X-ray Science Division
Advanced Photon Source
Argonne National Laboratory
9700 South Cass Avenue, Lemont, IL 60439, USA

Dr. A. Guda
The Smart Materials Research Institute
Southern Federal University
344090 Rostov-on-Don, Russia

carbides, oxides, phosphides, and borides).[4] These heterogeneous catalysts have been applied toward different energy applications such as HER, oxygen evolution reaction (OER), and oxygen reduction reaction (ORR) with limited electrochemical activity. On the other hand, layered transitions metal dichalcogenides have attracted much attention recently as effective electrocatalysts, where their active sites mostly localized at the surface or at the edges.[5]

Single atom catalysts (SACs) supported on a solid substrate can open up a new era in the field of heterogeneous catalysis research, offering a single active site with full atom utilization and high catalytic activity toward numerous chemical reactions.[6] On the other hand, the homogeneity of single atom sites eases more selectivity toward a specific product. However, the strong electronic or covalent interaction between single atom with its support makes it thermodynamically stable in the reaction process.[7] In an atomic level, some unique properties of SACs bring extraordinary reaction selectivity, activity, and stability over nanomaterials or clusters. A few of them are unsaturated coordination environment of metal active centers and quantum size effects, where electron confinement produces distinctive highest occupied molecular orbital (HOMO)–lowest unoccupied molecular orbital (LUMO) gap and discrete energy level, and finally strong metal–support interaction facilitates charge transfer between them.[8] Usually, SACs are supported on solid substrates to avoid aggregation, in which bulk metals and their oxides are widely used.[7d,9] However, the low conductivity and instability of these substrates in a harsh electrolytic environment (strong acid and base) force us to search for alternatives. Graphene, the world's first 2D material, is a potential candidate as the substrate, as it provides large surface area, high electrical conductivity, good stability, and high dispersion for electrocatalysts.[10] The performance of SACs largely depends on chemical bonding and charge transfer between atomically dispersed metal and substrate materials. Moreover, bonding strength can be increased by adding electron rich element like nitrogen into graphene (lone pair of nitrogen bonded with empty d-orbitals of transition metals), which eventually prevents metallic agglomeration.[8d,11] In addition, the development of modern experimental characterization techniques together with theoretical predictions has also played a crucial role in the development of SACs. However, among all transition metals, a few have been widely investigated as a SAC on nitrogen doped (N-doped) graphene substrate toward ORR,[12] OER,[13] HER,[14] and CO_2 reduction,[15] but their origin of activity still remains unclear. Furthermore, the relation among catalysts structure, electronic properties, and their activity has not yet been systematically studied for the design of highly efficient SACs for HER.

Herein, we used density functional theory (DFT) to calculate the catalytic activity for a series of transition metals embedded on N-doped graphene as SACs and found that Co-SAC exhibits highest activity. The activity of SACs for HER, originated from catalysts electronic structures, was correlated by investigating their density of state (DOS) profiles. We found that the energy level of the metallic valence d_{z^2} orbital and the antibonding orbital has largest impact on determining catalytic activity for HER. The position of the active valence d_{z^2} orbital is close to zero, which results in partially filled antibonding state orbital in the Co-SAC case, making it the most active for HER. Based on this finding, we derived correlation of the activity–electronic structure for all studied SACs, demonstrating the origin of hydrogen evolution activity. Guided by the calculated results, we synthesized three types of SACs, cobalt (Co-SAC), nickel (Ni-SAC), and tungsten (W-SAC), embedded on N-doped graphene substrate and investigated their atomic coordination and morphology by extended X-ray absorption fine structure (EXAFS), X-ray absorption near-edge structure (XANES), and direct imaging via annular dark-field scanning transmission electron microscope (ADF-STEM) characterizations. We found that single atoms were well separated and distributed uniformly throughout the whole graphene surface and existed as $M\text{-}N_4C_4$ moieties. We also compared their electrochemical activity for HER experimentally in acidic conditions and found that Co-SAC showed superior activity over others, which has shown good agreement with our theoretically derived activity–electronic structure correlation trends for SACs. Henceforth, we believe our derived linear activity–electronic structure correlation trend provides a better resolution toward the design of highly efficient SACs and gives deep insights in choosing the proper SAC for HER application.

2. Results and Discussion

2.1. Theoretical Activity Prediction of SACs for HER

Molecular hydrogen generation by the electrochemical reduction of hydrogen ion produced via water splitting is one of the most effective and cleanest technologies for future sustainable energy supply. HER is a combination of proton adsorption on catalyst surface via Volmer reaction ($H^+ + e^- + * \rightarrow H^*$, where * refers to catalysts surface) followed by desorption of H_2 through either Tafel reaction ($2H^* \rightarrow H_2 + 2^*$) or Heyrovsky reaction ($H^+ + e^- + H^* \rightarrow H_2 + {}^*$). The adsorption and desorption reactions compete on the catalyst surface, which can be illustrated using the Gibbs free energy calculation. The free energy change for hydrogen adsorption on the catalyst surface ($\Delta G_H{}^*$) determines the kinetics of the HER. According to Sabatier principle, when $\Delta G_H{}^*$ value is close to zero, the overall reaction rate for HER reaches maximum, expressed as in the form of "volcano plot" for various catalysts' surfaces.[16] From this, a good catalyst should form a bond with adsorbed H atom that is optimum for easy charge transfer and break readily to evolve as a hydrogen gas. If the interaction between H and catalyst is too strong, desorption reaction (Tafel/Heyrovsky) will be limited, while too weak interaction creates difficulty for Volmer reaction to proceed.[16,17] It has been reported experimentally that when SACs are synthesized on N-doped graphene substrate, the final product structure consists of several active nitrogen sites.[13–15,18] Based on these results we constructed a molecular model of SACs for hydrogen adsorption energy calculation including

Prof. Y. Hao
National Laboratory of Solid State Microstructures
College of Engineering and Applied Sciences
Collaborative Innovation Center of Advanced Microstructures,
and Jiangsu Key Laboratory of Artificial Functional Materials
Nanjing University
Nanjing 210093, China

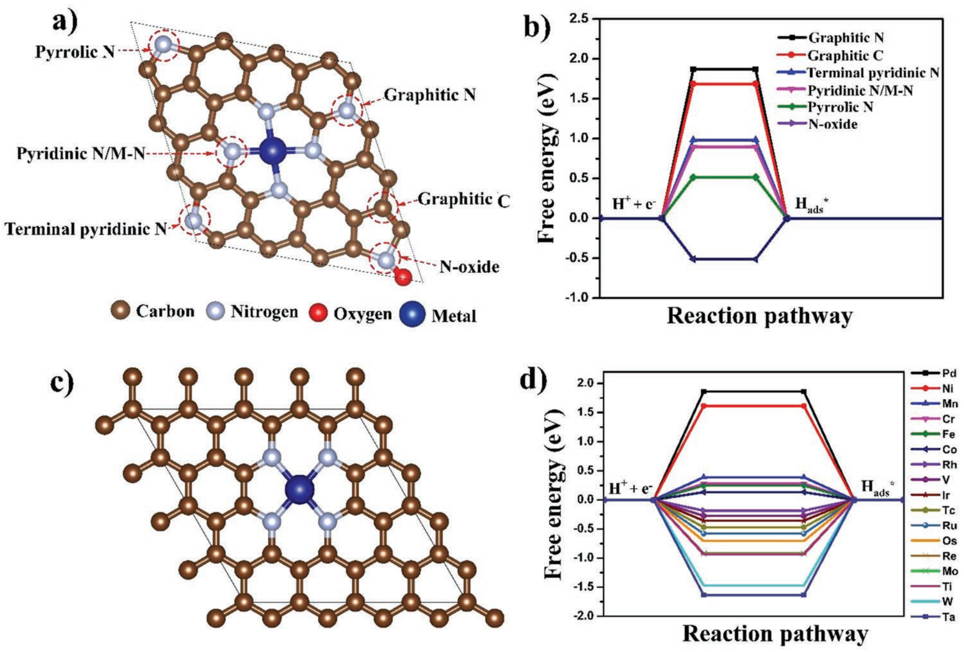

Figure 1. Proposed model of single atom catalysts and their Gibbs free energy calculation toward hydrogen adsorption reaction. a) Nonmetallic sites for hydrogen adsorption in the metal functionalized N-doped graphene. b) Gibbs free energies (ΔG_H*) for hydrogen adsorption reaction for each site. c) Metal active site coordinated with four nitrogen atoms in graphene sheet. d) Gibbs free energy (ΔG_H*) diagram for hydrogen adsorption reaction (Volmer reaction) toward a series of transition metals used as single atom catalysts.

all possible active sites, namely, graphitic-N, graphitic-C, pyridinic-N, terminal pyridinic-N, pyrrolic-N, and N-oxide species. **Figure 1**a shows the proposed molecular model for Gibbs free energy calculation for HER, constructed by considering all possible active sites for SACs on N-doped graphene surface. To determine the substrate activity, we calculated Gibbs free energy for hydrogen adsorption on the abovementioned sites (Figure S1, Supporting Information) of SAC and plotted in Figure 1b. The figure shows that none of the studied sites are electrochemically active, as their Gibbs free energies are high. Based on their catalytic activity, we summarized them into the following order: N-oxide species (–0.51 eV) > pyrrolic N (0.52 eV) > pyridinic N/M-N (0.89 eV) > terminal graphitic N (1.01 eV) > graphitic C (1.69 eV) > graphitic N (1.89 eV). The latter two sites, graphitic-N and graphitic-C showed very high positive ΔG_H* values, indicating complete inhibition of hydrogen adsorption step for HER. Since functionalization of graphene with metal as SAC offers single active site as well as full atomic utilization for catalytic reaction, we considered a molecular model as a metal active site for further calculations, as shown in Figure 1c. The model represents transition metal atom (partially empty orbital) coordinated with four nitrogen atoms (lone pair electrons) forming strong covalent bond embedded on graphene structure. As nitrogen bonded with metal through their lone pair electrons, their hybrid electronic properties have a potential effect on the activity of HER. We then studied the Gibbs free energy by changing the central metal atom (Figure 1c) on N-doped graphene skeleton for a series of transition metal as SACs, as summarized in Figure 1d. This diagram demonstrates that not every type of single atom exhibits activity toward HER. However, Co-SAC (ΔG_H* = 0.13) shows higher activity among all SACs studied. We found that Pd-SAC and Ni-SAC had very weak interactions with hydrogen as their Gibbs free energy is very high (ΔG_H* = 1.86 and 1.62 eV, respectively) while Re-SAC, Mo-SAC, Ti-SAC, W-SAC, and Ta-SAC exhibited very high negative Gibbs free energy (–0.92, –0.93, –0.94, –1.44, and –1.64 eV, respectively) indicating strong attraction for hydrogen. As in case of SACs, the active site (metal) lies on the surface (nonedge side) of graphene, therefore, we proposed the HER mechanism by considering Volmer–Heyrovsky pathways (Figure S2, Supporting Information) rather than the Volmer–Tafel pathways designed for edge side hydrogen adsorption.[19]

2.2. SACs Design Principle Based on the Origin of Activity

To rationally design highly efficient electrocatalysts for HER, we carried out DFT calculations to elucidate the electronic properties of metal hybrid orbitals and their correlation with HER activity (ΔG_H*) with the help of d-band theory,[20] as shown in **Figure 2**a. Schematically, when hydrogen is adsorbed on the catalysts surface, the active valence orbitals of catalysts (wooden color) interact with hydrogen orbital (gray) and produce two orbital states (blue). One is partially filled electronic orbital (partial blue), forming antibonding state (σ*) orbital while another (blue) forms bonding state (σ) orbital. To find the origin of activity, the total density of states and projected density of states (PDOS) were calculated for all individual atoms in the Co-SAC structure (Figure S3, Supporting Information), while the PDOS of 3d orbitals for Co-SAC before and after interaction with hydrogen is shown in Figure 2b. A few of the orbitals of intake catalysts disappeared as well as some new

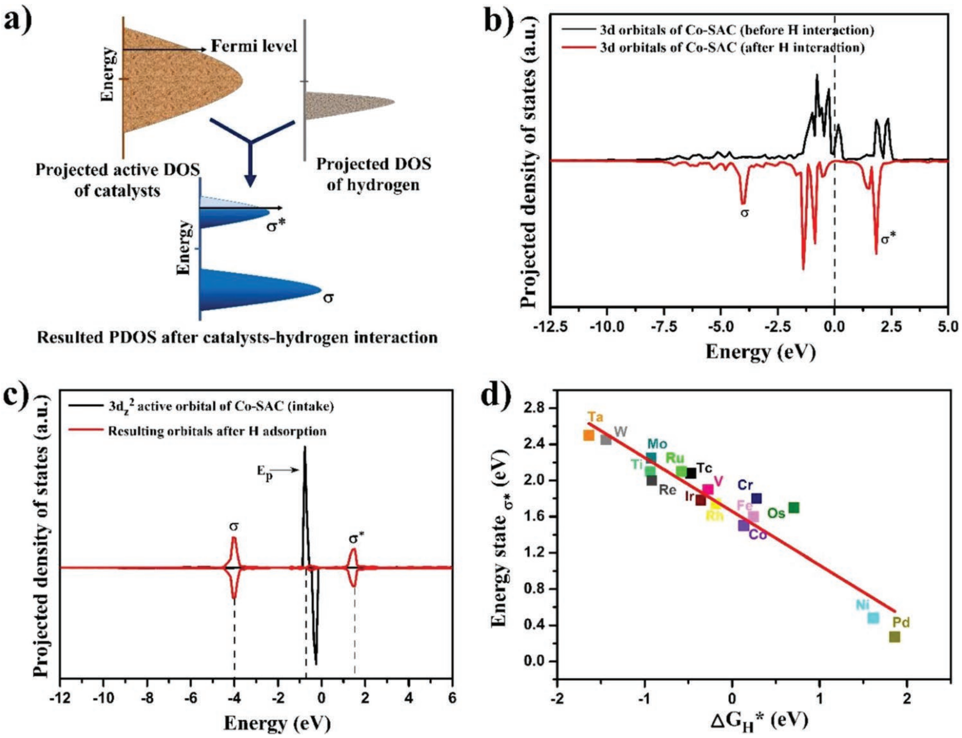

Figure 2. Electronic structure of single atom catalysts and their activity relation. a) Scheme of orbital hybridization of catalysts active sites with hydrogen (σ = bonding, and σ^* = antibonding state orbital). b) Projected DOS of 3d hybrid orbital of Co-SAC before and after hydrogen interaction. c) The PDOS for 3d$_{z^2}$ active orbital (E_p, spin-up and spin down) of Co-SAC interacts with hydrogen and produces σ and σ^* orbitals. d) Correlation between Gibbs free energy (ΔG_H*) and antibonding state, E_{σ^*} across the fermi level originated from the interaction of active valence d$_{z^2}$ orbital of single atom catalysts with hydrogen atom.

orbital peaks evolved after interacting with hydrogen. These new peaks are designated as bonding (σ) and antibonding (σ^*) orbitals in Figure 2a. As the electrons in single atom catalysts discrete into various individual energy levels due to quantum size effects, it is very convenient for hydrogen to interact with specific metallic orbital for reaction without disturbing others. To proof our assumptions and get more deeper scenario, we calculated the PDOS of individual states of cobalt 3d orbitals in Co-SAC before and after hydrogen adsorption and found that not every orbital is taking part in the reaction (Figure S4, Supporting Information). However, we identified only 3d$_{z^2}$ valence orbital (spin-up and spin-down) is actively participating in the hybridization with hydrogen for Co-SAC represented in Figure 2c. The active valence 3d$_{z^2}$ orbitals (E_p) were converted into two different orbitals, where one goes across the Fermi level (antibonding state orbital, σ^*) and other lies below (bonding state orbital, σ), as shown in Figure 2a. Similarly, we calculated the PDOS for all studied SACs and found similar hybridization like Figure 2c. Since, the d$_{z^2}$ valence orbital of each SAC participates in the bond formation with hydrogen and produces bonding and antibonding states, we identified these three orbital states (E_p, σ, σ^*) as activity descriptor for HER. The distinctive electronic structure of SACs helps to explain the origin of electrochemical activity much more easily than in case of nanoparticles or metal clusters. To explore the activity relation, we plotted these activity descriptors against the corresponding value of Gibbs free energy ΔG_H* for all SACs. Among three, the antibonding energy states (E_{σ^*}) for all SACs show best linear correlation with ΔG_H*, as shown in Figure 2d. This figure implies that the location of antibonding states (E_{σ^*}) in case of Ta-SAC and W-SAC moved higher energy level with a lower occupancy, ensuring strong interaction with hydrogen (high negative ΔG_H*), while an increased filling of antibonding states was observed in cases of Ni-SAC and Pd-SAC, resulting in diminishing activity toward HER. Therefore, higher the location means empty antibonding state results strong interaction and vice versa. We also correlated the relationship among active valence d$_{z^2}$ energy state (E_p, normally bigger peak) and bonding energy state (E_σ) with Gibbs free energy (ΔG_H*) for all studied SAC models (Figures S5–S8, Supporting Information). We found that lower valence d$_{z^2}$ orbital resulted weaker interaction while higher valence d$_{z^2}$ ensured stronger interaction. The position of active valence d$_{z^2}$ orbital (E_p) near to Fermi level produced partially filled antibonding state (E_{σ^*}), suggesting ideal situation ($\Delta G_H^* \approx 0$) for the design of SACs in case of HER.

As charge transfer quantifies the bonding strength between adsorbate and catalysts, we calculated and depicted the charge transfer scenario for Ta-SAC-H model in **Figure 3**a. The Bader charge profile for the Ta-SAC-H system shows a maximum charge transfer (0.84 e$^-$/H atom) to hydrogen, resulting in strong binding energy ($\Delta G_H^* = -1.64$ eV). Similarly, Pd-SAC transfers very little charge (0.10 e$^-$/H atom) to hydrogen during adsorption owing to very little catalytic activity ($\Delta G_H^* = 1.86$ eV), while Cr-SAC shows an intermediate amount of charge transfer (0.42 e$^-$/H atom) with relatively better HER activity ($\Delta G_H^* = 0.28$ eV) (Figure S9, Supporting Information).

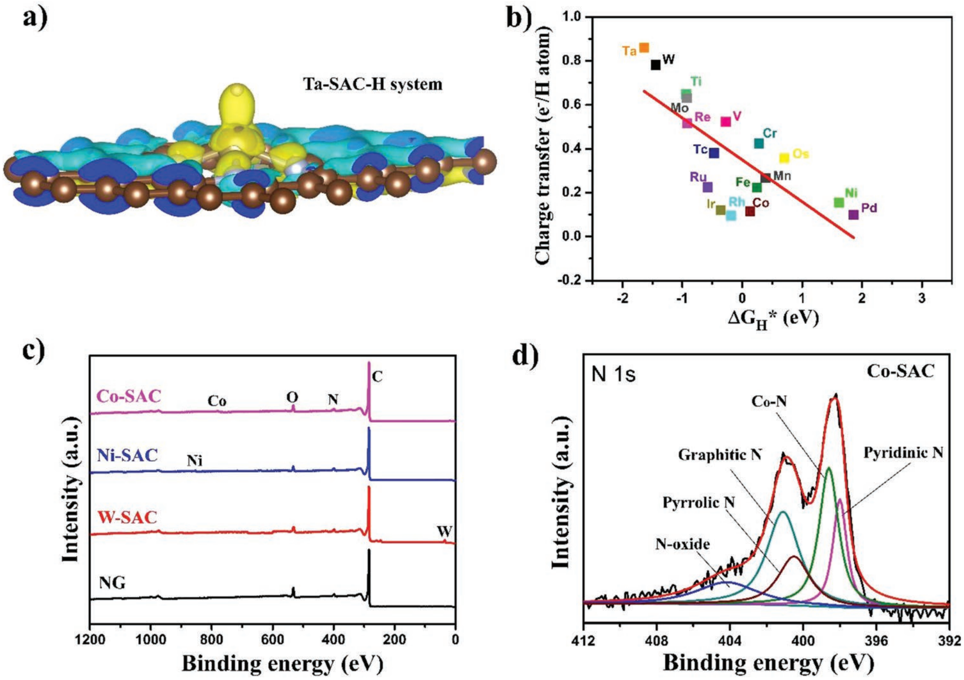

Figure 3. Charge transfer and chemical composition of single atom catalysts. a) Charge transfer from Ta-SAC to hydrogen during the reaction (yellow color represents electron availability while blue is for electron deficiency, isosurface value = 0.022156 e Å^{-3}). b) Relationship between charge transfer and HER activity (Gibbs free energy). c) XPS spectra of Co, Ni, and W single atom catalyst together with control nitrogen doped graphene (NG). The very weak peak of metal atoms confirmed the presence of very fraction amount of metal in the catalysts composition. d) N 1s deconvoluted spectra for cobalt single atom (Co-SAC), representing all predicted nitrogen active sites are present in the catalysts structure.

To configure the activity relation with the charge transfer, we derived a correlation for a series of SACs, as shown in Figure 3b. We have found that maximum SACs followed the charge transfer-Gibbs free energy (ΔG_H*) linear trends while few of them (Ru, Rh, Ir, Co) were slightly deviated. As Gibbs free energy (ΔG_H*) is the indication of the electrochemical activity for a catalyst, so we think Ir-SAC and Co-SAC still be catalytically active as their ΔG_H* value is close to zero. Finally, this linear relationship between the amount of charge transfer and Gibbs free energy (ΔG_H*) suggests an ideal charge transfer (0.35 e$^-$/H atom approximately) to design a highly active SAC (ΔG_H* = 0 eV) for HER. On the basis of our theoretical hypothesis, we synthesized three kinds of single atom (Co, Ni, and W) catalysts using graphene oxide (GO), acrylamide, and metallic chloride salts (details in the Experimental Section) as precursors. The compositions and chemical states of prepared SACs supported on N-doped graphene were studied with the X-ray photoelectron spectroscopy (XPS) shown in Figure 3c,d, respectively. Figure 3c represents the elemental analysis for all three SACs together with the control sample (N-doped graphene, NG). The XPS results show a very tiny peak for metals, indicating a fraction of amount of metal atoms exist together with O, N, and C in the prepared SAC sample (Figure S10, Supporting Information). The metals (Co, Ni, and W) existed in the catalysts with mixture of two valence states as compared to their pure and oxide states, confirmed by the high-resolution peak spectrum (Figure S11, Supporting Information). To identify different types of nitrogen active sites in the SACs, we deconvoluted N 1s peak into several peaks for Co-SAC, shown in Figure 3d. It shows that the N 1s peak for Co-SAC deconvoluted into pyridinic N (398.0 eV), Co—N (398.6 eV), pyrrolic N (400.5 eV), graphitic N (401.1 eV), and N-oxide (404.2 eV).[14b] The slight binding energy difference between pyridinic N and Co—N is showed that they are well separated from each other. Similarly, all the nitrogen active sites used for theoretical calculation were also confirmed for W-SAC and Ni-SAC alone with the control sample (NG) (Figure S12, Supporting Information).

2.3. Structural and Electrochemical Characterization

The electronic states and atomic configuration of the metal embedded as a single atom in N-doped graphene frameworks were further investigated with the XANES and EXAFS. The metal K-edge XANES and EXAFS spectra for Co-SAC, Ni-SAC, and L_3-edge of W-SAC are summarized in **Figure 4** with their respective bulk metal and oxide refs. [13,14b,15,21]. Figure 4a represents XANES spectra for Co-SAC indicating that the local atomic structure around Co in Co-SAC was significantly different from bulk Co and CoO. This is more clearly observed from its first derivative curves (insets) suggesting intermediate oxidation states in Co-SAC. However, enhanced pre-edge feature and shoulder arising due to 1s→3d and 1s→4pz transitions correspondingly can be explained also by planar geometry of the complex compared to octahedral structure of CoO. Taking into account the XPS results in the different oxidation state of Co atoms in Co-SAC due to the existence of Co-N_4C_4 moiety via N-coordination bond with Co. Similar behavior is also observed for Ni-SAC and W-SAC cases, where Figure 4b,c shows that the XANES spectra for Ni-SAC and W-SAC were not overlapped

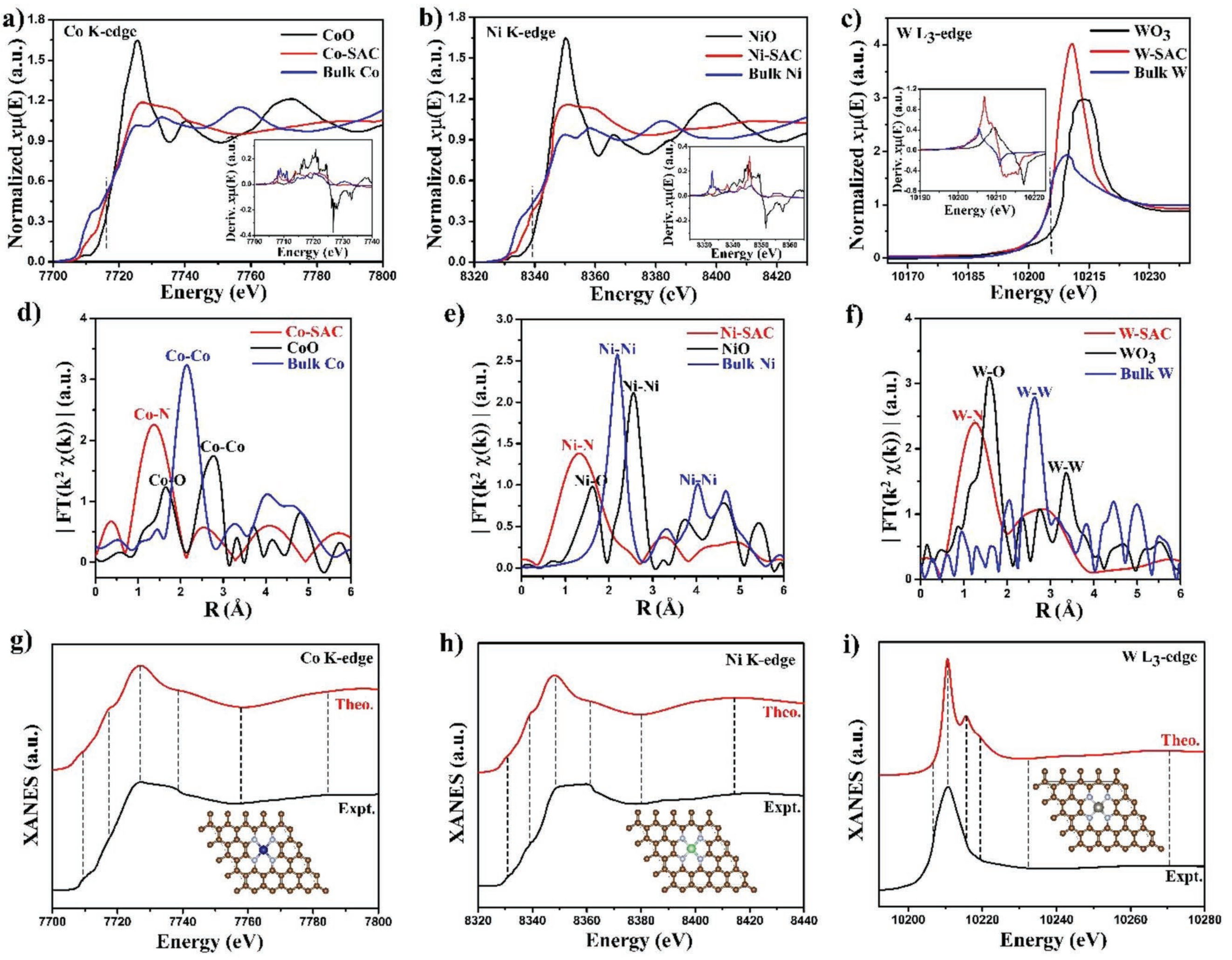

Figure 4. Structural and chemical states information of SACs revealed by EXAFS and XANES characterization. Experimental XANES spectra for a) Co K-edge for Co-SAC, b) Ni K-edge for Ni-SAC, c) W L_3-edge for W-SAC and first derivative curves (insets) with their reference samples (bulk metal and metal oxide). Fourier transform (FT) magnitudes of EXAFS spectra in R space of d) Co-SAC, e) Ni-SAC, and f) W-SAC with their bulk and oxide states respectively. g–i) Relative comparison between experimentally obtained XANES spectra with the theoretically derived one based on M-N_4C_4 moieties embedded in the graphene structure (insets).

with their bulk and oxide references indicating differences in metal coordination from the closed packed structure of references. Both 1s→3d and 1s→4pz peak intensities are higher for Ni-SAC than for NiO, similar things (2p→5d and 2p→6pz) happened for W-SAC. The differences in intensity of the main edge peaks in case of SACs are confirmed by the existence of divacancy based M-N_4C_4 moieties bonded axially with broken D_{4h} symmetry.[13,22]In addition, the bonding and coordination environment around metal in the SACs were further studied with the EXAFS Fourier transform (FT) for all three SACs shown in Figure 4d–f. Figure 4d shows that the EXAFS FT spectra of Co-SAC exhibits a major peak at around 1.43 Å, which is different from Co—O peak at 1.63 Å and Co—Co peaks at 2.1 and 2.7 Å, respectively, corresponding to Co—N bonding.[13,14b,23] Similarly, Figure 4e,f shows EXAFS FT spectra for Ni-SAC and W-SAC exhibit major peaks at 1.44 and 1.45 Å, respectively, that were different from the peaks for Ni—O (at 1.62 Å), Ni—Ni (2.20 and 2.60 Å), W—O (1.60 Å), and W—W (2.6 and 3.40 Å), attributed for Ni—N and W—N bond, respectively[15,21a,24] Finally, for more confirmation about SACs structure, we calculated XANES spectra for SACs theoretically by means of accurate finite difference approach implemented in FDMNES software. Results of these calculations are shown in Figure 4g–i. Figure 4g–i shows the comparison of experimental XANES spectra with theoretically calculated XANES spectra obtained from energetically relaxed SAC molecular models (insets). The theoretically simulated XANES spectra for all three SACs showed similar behavior (edge position and shapes) to experimental data. Depending on the XANES, EXAFS, and FDMNES results, we concluded that our theoretical model based on M-N_4C_4 moieties on graphene structure is very practical and could be applied to direct design of SACs for many general fields of electrochemistry.

The atomic structure of SACs was further examined by ADF-STEM. **Figure 5**a shows the STEM image of W-SAC where the atomic form of metals (white dots) is seen to distribute homogeneously throughout the whole graphene matrix

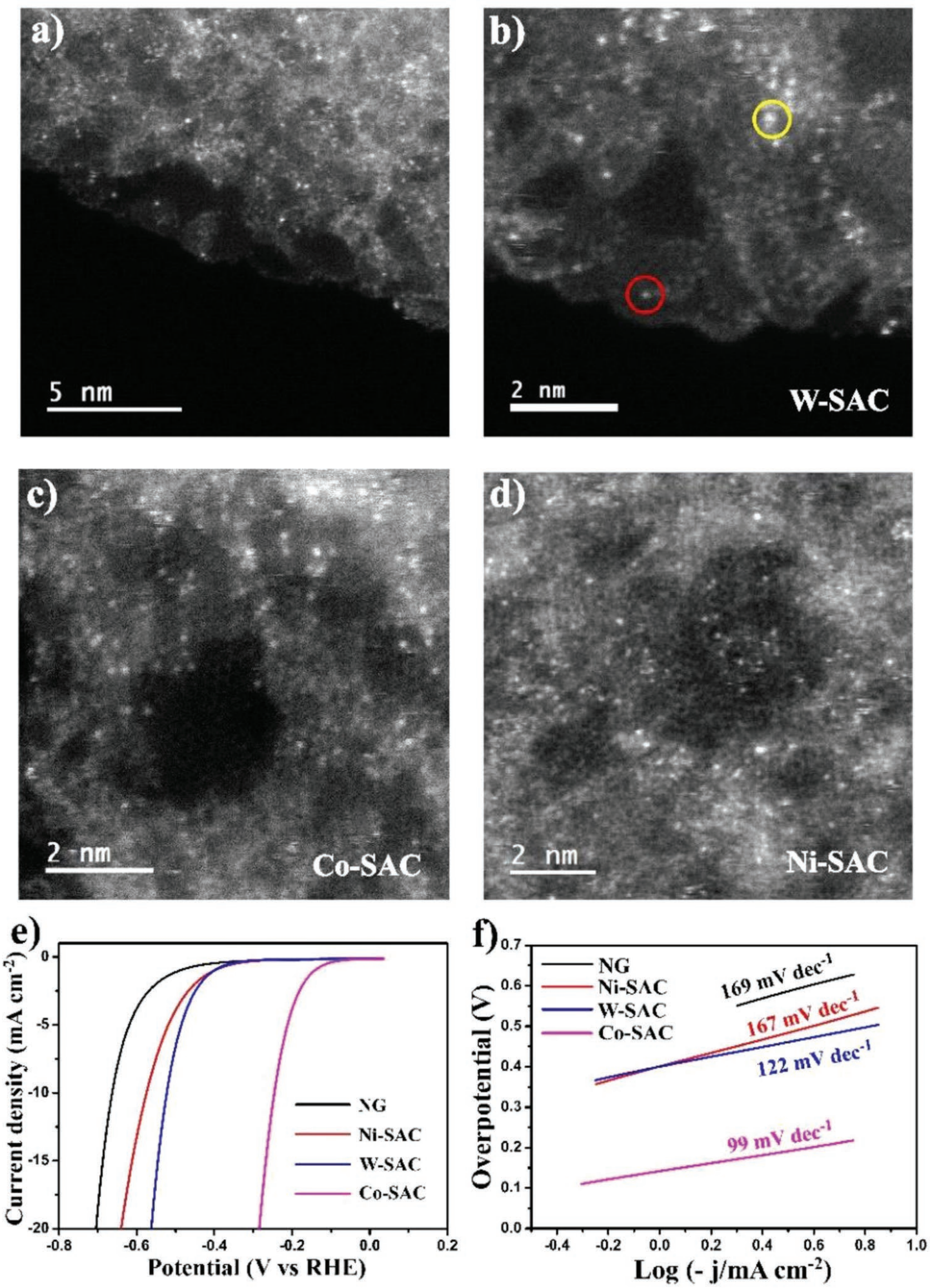

Figure 5. STEM and electrochemical characterization. a) Isolated tungsten single atom (bright dots) uniformly distributed throughout the whole graphene surface unraveled by ADF-STEM image. b–d) STEM images of W-SAC, Co-SAC, and Ni-SAC, respectively, at higher magnification. The single atoms marked by red and yellow circles in (b) indicating they were evenly dispersed in monolayer and multilayer graphene matrix respectively. e) Linear sweep voltammetry curves of SACs for HER alone with control sample (NG) are obtained in 0.5 M H_2SO_4 at a scan rate of 10 mV s^{-1}. f) Corresponding Tafel plots for the HER polarization curves in (e).

(Figures S13–S18, Supporting Information). The size of each dot is ≈2–3 Å. The atomic resolution STEM images are presented in Figure 5b–d, respectively. The single atoms in each SAC located on the monolayer and multilayer graphenes were indicated by red and yellow circles, respectively. In all three SACs, the presence of the single atom was further confirmed by electron energy loss spectra (EELS) characterization (Figures S19–S21, Supporting Information). The single atoms in each case were well separated from each other and existed similarly as M-N_4C_4 moieties previously revealed by the EXAFS study.

Furthermore, the hydrogen evolution catalytic activity of the synthesized SACs was examined to verify our computational results. HER activities were studied in an electrochemical cell with a three-electrode system using 200 µg cm^{-2} catalyst mass loading on glassy carbon. The linear sweep voltammograms for HER activity are shown in Figure 5e, obtained at a scan rate of

10 mV s^{-1} in 0.5 M H_2SO_4 after iR compensation. The polarization curves demonstrate that Co-SAC had greater electrolytic activity toward HER as compared to Ni-SAC, W-SAC, and the control sample. In addition, the overpotentials needed to produce 10 mA cm^{-2} current density for HER were 230, 530, 590, and 630 mV (vs RHE) in case of Co-SAC, W-SAC, Ni-SAC, and NG, respectively. This result is in agreement with our calculated Gibbs free energy trend (Figure 1d). The Tafel slopes of the polarization curves were then plotted in Figure 5f, which shows that Co-SAC had a smaller Tafel slope (99 mV dec^{-1}) with higher exchange current density (3.88×10^{-2} mA cm^{-2}) (Figure S22, Supporting Information) as compared to W-SAC (122 mV dec^{-1}), Ni-SAC (167 mV dec^{-1}), and NG (169 mV dec^{-1}). To investigate the long-term stability, we carried out cyclic voltammetry (CV) experiments for Co single atom catalysts in acidic conditions. The polarization curves obtained from CV show an insignificant decrease in performance even after 1000 cycles (Figure S23, Supporting Information), confirming the long-term stability of this catalyst.

3. Conclusion

In this work, we derived an activity–electronic structure relationship to explore the origin of hydrogen evolution activity for a series of transitional metals as single atom catalyst with the help of density functional theory. The calculated Gibbs free energy indicated that Co-SAC shows greater activity among all studied SACs. DOS calculation has shown that only the valence $d_z{}^2$ orbital actively participates in the reaction with hydrogen. The energy states of valence $d_z{}^2$ and its antibonding orbital are highly correlated with catalytic activity, ΔG_H*. The higher energy level of antibonding state results in fully unoccupied orbital certifying strong interaction with hydrogen and vice versa. The superior electrochemical activity of Co-SAC toward HER was mainly due to the location of $3d_z{}^2$ valence orbital near to the Fermi level, and its partially empty antibonding state, ensuring optimum adsorption strength toward hydrogen adsorption than others. Moreover, we found linear correlation for the catalytic activity (ΔG_H*) with electronic structure (E_p and $E_{\sigma*}$) of SACs and charge transfer along SACs. To verify our computational results, three SACs (Co, Ni, W) were synthesized and they all show that the isolated single atoms are distributed homogeneously over N-doped graphene surface as $M\text{-}N_4C_4$ moieties, clearly identified by EXAFS, XANES, and STEM characterizations. Moreover, our experimental result shows that Co-SAC has superior activity toward HER over Ni-SAC and W-SAC. This electrochemical performance of the SACs exhibits in accordance results with our theoretical derived activity trends. Our derived relationship is a potential solution to the problems of designing highly efficient SACs for HER application and adding a new chapter in the development of future energy conversion technology.

4. Experimental Section

Computational Methods: The catalytic activity and electronic structure of SACs were investigated by considering spin polarization DFT calculation, using projector augmented wave pseudopotentials[25] and the Perdew–Burke–Ernzerhof exchange–correlation functional within the generalized gradient approximation[26] as implemented in the Vienna ab initio package code.[27] For electron wave expansion, a plane wave of 500 eV cutoff energy was set. The structure relaxation energy criteria were set to be 10^{-6} eV, while forces for each atom were less than 0.01 eV $Å^{-1}$. A Gaussian smearing of 0.05 eV was applied throughout the whole calculation. The K-points were selected to be 9 × 9 × 1 for structure relaxation and energy calculation, while for electronic structure calculation the denser 45 × 45 × 1 K-points were used. 4 × 4 super cells of graphene were used with 26 carbon atoms and 1 metal atom placed on carbon divacancy that were bonded with 4 nitrogen atoms. The unit cell dimensions were optimized to 2.46 × 2.46 with a distance of 20 Å between the two layers in a periodic condition.

Gibbs Free Energy and Charge Transfer Measurements: The hydrogen evolution reaction involves the adsorption of proton on the catalysts surface followed by the generation of molecular hydrogen through desorption. The optimum adsorption energy should neither be too high nor too low. The hydrogen adsorption energy on SACs surface is calculated by the following equation

$$\Delta E_{\text{ad}} = E_{\text{SACs}-\text{H}*} - E_{\text{SACs}} - \frac{1}{2}E_{\text{H}_2} \quad (1)$$

where $E_{\text{SACs-H}*}$ is the total energy of single atom catalysts with adsorbed H state, E_{SACs} is the energy of single atom catalyst surface, and E_{H2} is the energy of hydrogen in the gas phase. For the best catalyst, Gibbs free energy ($\Delta G_{\text{H}*}$) should be close to zero. Gibbs free energy was calculated by considering zero-point energy (ZPE) and entropy corrections for hydrogen evolution reaction as per the following equation

$$\Delta G_{\text{H}*} = \Delta E_{\text{ad}} + \Delta E_{\text{ZPE}} - T\Delta S \quad (2)$$

The hydrogen adsorption energy on catalysts surface is denoted by ΔE_{ad}, while the difference in zero-point energy and entropy between the adsorbed and gaseous hydrogen is represented by ΔE_{ZPE} and ΔS. In adsorbed state, hydrogen shows negligible entropy change due to vibrational force, so the Gibbs free energy is calculated by considering the following corrections[16]

$$\Delta G_{\text{H}*} = \Delta E_{\text{ad}} + 0.24\text{eV} \quad (3)$$

The Bader charge analysis was carried out to estimate the charge transfer quantitatively between catalysts and hydrogen using a method developed by the Henkelman et al.[28] The charge transfer profile was visualized using a free VESTA software.

Synthesis of SACs: All chemicals with analytical grade were purchased from Sigma-Aldrich and deionized (DI) water was used throughout the whole work. GO suspension with 4 mg mL^{-1} concentration was prepared from graphite flakes (average particle size of 350 nm) according to the modified Hummers method[29] reported in the previous work.[4c] Three different types of single atom catalysts were synthesized, namely, Ni-SAC, Co-SAC, and W-SAC, separately alone with nitrogen doped graphene (control sample) in order to compare their electrochemical HER activity in acidic solution. For the metal precursor, $NiCl_2.6H_2O$ (0.05 M Ni^{2+}), $CoCl_2.6H_2O$ (0.05 M Co^{2+}), WCl_6 (0.05 M W^{6+}) salts were used. GO suspension was diluted by mixing 2.5 mL of 4 mg mL^{-1} GO into 30 mL DI water. Accurately measured 25 µL of 0.05 M Ni^{2+} solution and 100 µL acrylamides (25 wt%, as a nitrogen precursors) were added into the diluted GO suspension and stirred for 24 h. The mixed solution was freeze-dried for another 24 h. The brownish freeze-dried sample was annealed in 1 inch quartz tube furnace at 750 °C for 1 h under Ar (100 s.c.c.m) atmosphere to produce Ni-SAC. Similarly, Co-SAC and W-SAC were prepared by using equimolar (25 µL) amount of Co^{2+} and W^{6+} solutions instead of Ni^{2+} precursor in the abovementioned procedure. The control sample was prepared without the addition of a metal precursor. The prepared SACs were then acid leached at 80 °C for 24 h, followed by heating at 750 °C for 1 h to regain its crystallinity after washing with DI water.

Catalysts Characterization: The chemical composition and elemental oxidation state of SACs were investigated using the XPS with Kratos Axis Ultra DLD spectrometer. X-ray absorption spectroscopy (XAS) experiments on Ni K-edge, Co K-edge, and W L_3-edge were conducted in fluorescence mode at beamlines 20-BM-B and 9-BM-B of the Advanced Photon Source (APS) at Argonne National Laboratory, using a Si (111) double crystal monochromator. The applied electron energy and current were 7 GeV and 100 Ma, respectively. The data obtained from XAS were processed and analyzed using the ATHENA program.[30] The theoretical XANES spectra for Co, Ni K-edge, and W L_3-edge were obtained by using the FDMNES code with infinite difference approximation.[31] The structures used for FDMNES were previously optimized using the DFT calculation. The morphology and elemental mapping of SACs were characterized with the transmission electron microscopy JEM-2800. The single atom in the SACs was further investigated by ADF-STEM and core-loss EELS using the Nion Ultra STEM 200 at UC, Irvine, equipped with C3/C5 corrector and high-energy resolution monochromated EELS system. The instrument was operated at 60 kV with a convergence semiangle of 30 mrad. For STEM imaging, the inner and outer collection semi-angles of ADF detector were 50 and 210 mrad, respectively. For core-loss EELS measurement, a dispersion of 0.6 eV per channel was used and the dwell time was 5 s per spectrum. The background in each spectrum was removed by the power-law function in the commercial software package Digital Micrograph.

Electrochemical Characterizations: The hydrogen evolution reaction experiments were carried out in an electrolytic cell (CHI 760C workstation) with three electrode systems in 0.5 M H_2SO_4 and room temperature. Saturated Ag/AgCl (sat. KCl) and platinum wire were used as reference and counter electrodes, respectively. The working electrode was prepared by dispersing 2 mg of catalysts and 20 µL Nafion into 2 mL of 4:1 (v/v) water/isopropanol for 60 min by sonication. About 39.9 µL homogeneous solution was loaded onto the 5 mm diameter of glassy carbon (mass loading ≈ 0.200 mg cm^{-2}) and then, linear sweep voltammetry was carried out from –0.2 to 0.9 V with 10 mV s^{-1} scan rate. Long-term stability tests were performed in 0.5 M H_2SO_4 at room temperature by potential cycling between 0.0 and –0.6 V (vs Ag/AgCl) at a potential sweep rate of 50 mV s^{-1} for a given number of cycles. For all experiments, the catalyst mass loading was kept constant (0.200 mg cm^{-2}) and all polarization curves were taken after iR compensation.

Supporting Information

Supporting Information is available from the Wiley Online Library or from the author.

Acknowledgements

This project was supported by the Research Grant Council of Hong Kong SAR (Project number 16204815), NSFC-RGC Joint Research Scheme (N_HKUST607/17), the Innovation and Technology Commission (ITC-CNERC14SC01), the Guangzhou Science & Technology (Project 201704030134). X.Y., C.A.G. and X.P. thank the support of the University of California, Irvine Materials Research Institute for the use of TEM facilities. This research used resources of the Advanced Photon Source, an Office of Science User Facility operated for the U.S. Department of Energy (DOE) Office of Science by Argonne National Laboratory and was supported by the U.S.DOE under Contract No. DE-AC02-06CH11357, and the Canadian Light Source and its funding partners. A.A.G. Acknowledges a grant from the Southern Federal University (VnGr-07/2017-08) for financial support. The DFT calculations were performed on high performance computing facility funded by the School of Engineering, at HKUST. Technical assistance from the Materials Characterization and Preparation Facilities, HKUST, is greatly appreciated.

Conflict of Interest

The authors declare no conflict of interest.

Keywords

charge transfer, density functional theory, density of states, hydrogen evolution reaction, single atom catalysts

Received: November 28, 2018
Revised: January 2, 2019

---

[1] a) S. Chu, A. Majumdar, *Nature* **2012**, *488*, 294; b) Z. W. Seh, J. Kibsgaard, C. F. Dickens, I. Chorkendorff, J. K. Nørskov, T. F. Jaramillo, *Science* **2017**, *355*, eaad4998.

[2] a) J. Luo, J.-H. Im, M. T. Mayer, M. Schreier, M. K. Nazeeruddin, N.-G. Park, S. D. Tilley, H. J. Fan, M. Grätzel, *Science* **2014**, *345*, 1593; b) G. W. Crabtree, M. S. Dresselhaus, M. V. Buchanan, *Phys. Today* **2004**, *57*, 39; c) K. M. K. Yu, W. Tong, A. West, K. Cheung, T. Li, G. Smith, Y. Guo, S. C. E. Tsang, *Nat. Commun.* **2012**, *3*, 1230.

[3] a) J. A. Turner, *Science* **2004**, *305*, 972; b) J. G. N. Thomas, *Trans. Faraday Soc.* **1961**, *57*, 1603; c) Y. Zheng, Y. Jiao, Y. Zhu, L. H. Li, Y. Han, Y. Chen, A. Du, M. Jaroniec, S. Z. Qiao, *Nat. Commun.* **2014**, *5*, 3783; d) H. Yin, S. Zhao, K. Zhao, A. Muqsit, H. Tang, L. Chang, H. Zhao, Y. Gao, Z. Tang, *Nat. Commun.* **2015**, *6*, 6430.

[4] a) M. Cabán-Acevedo, M. L. Stone, J. R. Schmidt, J. G. Thomas, Q. Ding, H.-C. Chang, M.-L. Tsai, J.-H. He, S. Jin, *Nat. Mater.* **2015**, *14*, 1245; b) H. B. Wu, B. Y. Xia, L. Yu, X.-Y. Yu, X. W. Lou, *Nat. Commun.* **2015**, *6*, 6512; c) M. Zhuang, X. Ou, Y. Dou, L. Zhang, Q. Zhang, R. Wu, Y. Ding, M. Shao, Z. Luo, *Nano Lett.* **2016**, *16*, 4691; d) J. Duan, S. Chen, B. A. Chambers, G. G. Andersson, S. Z. Qiao, *Adv. Mater.* **2015**, *27*, 4234; e) H. Vrubel, X. Hu, *Angew. Chem., Int. Ed.* **2012**, *51*, 12703.

[5] a) A. T. Bell, *Science* **2003**, *299*, 1688; b) M. Zhuang, L.-Y. Gan, M. Zou, Y. Dou, X. Ou, Z. Liu, Y. Ding, I. H. Abidi, A. Tyagi, M. Jalali, J. You, A. Cao, Z. Luo, *J. Mater. Chem. A* **2018**, *6*, 2900; c) M.-R. Gao, Y.-F. Xu, J. Jiang, S.-H. Yu, *Chem. Soc. Rev.* **2013**, *42*, 2986.

[6] Y. Chen, S. Ji, C. Chen, Q. Peng, D. Wang, Y. Li, *Joule* **2018**, *2*, 1242.

[7] a) H. Zhang, G. Liu, L. Shi, J. Ye, *Adv. Energy Mater.* **2018**, *8*, 1701343; b) Y. Zhai, D. Pierre, R. Si, W. Deng, P. Ferrin, A. U. Nilekar, G. Peng, J. A. Herron, D. C. Bell, H. Saltsburg, M. Mavrikakis, M. Flytzani-Stephanopoulos, *Science* **2010**, *329*, 1633; c) H. Yan, H. Cheng, H. Yi, Y. Lin, T. Yao, C. Wang, J. Li, S. Wei, J. Lu, *J. Am. Chem. Soc.* **2015**, *137*, 10484; d) J. Jones, H. Xiong, A. T. DeLaRiva, E. J. Peterson, H. Pham, S. R. Challa, G. Qi, S. Oh, M. H. Wiebenga, X. I. Pereira Hernández, Y. Wang, A. K. Datye, *Science* **2016**, *353*, 150.

[8] a) R. Van Hardeveld, F. Hartog, *Surf. Sci.* **1969**, *15*, 189; b) P. Hu, Z. Huang, Z. Amghouz, M. Makkee, F. Xu, F. Kapteijn, A. Dikhtiarenko, Y. Chen, X. Gu, X. Tang, *Angew. Chem., Int. Ed.* **2014**, *53*, 3418; c) M. Valden, X. Lai, D. W. Goodman, *Science* **1998**, *281*, 1647; d) C. T. Campbell, *Nat. Chem.* **2012**, *4*, 597.

[9] a) M. Yang, L. F. Allard, M. Flytzani-Stephanopoulos, *J. Am. Chem. Soc.* **2013**, *135*, 3768; b) P. Liu, Y. Zhao, R. Qin, S. Mo, G. Chen, L. Gu, D. M. Chevrier, P. Zhang, Q. Guo, D. Zang, B. Wu, G. Fu, N. Zheng, *Science* **2016**, *352*, 797; c) J. Lin, A. Wang, B. Qiao, X. Liu, X. Yang, X. Wang, J. Liang, J. Li, J. Liu, T. Zhang, *J. Am. Chem. Soc.* **2013**, *135*, 15314.

[10] a) M. Liu, R. Zhang, W. Chen, *Chem. Rev.* **2014**, *114*, 5117; b) Y. Li, H. Wang, L. Xie, Y. Liang, G. Hong, H. Dai, *J. Am. Chem. Soc.* **2011**,

133, 7296; c) Y. Liang, Y. Li, H. Wang, H. Dai, *J. Am. Chem. Soc.* **2013**, *135*, 2013.
[11] a) B. Yoon, H. Häkkinen, U. Landman, A. S. Wörz, J.-M. Antonietti, S. Abbet, K. Judai, U. Heiz, *Science* **2005**, *307*, 403; b) N. Cheng, S. Stambula, D. Wang, M. N. Banis, J. Liu, A. Riese, B. Xiao, R. Li, T.-K. Sham, L.-M. Liu, G. A. Botton, X. Sun, *Nat. Commun.* **2016**, *7*, 13638.
[12] C. Zhang, J. Sha, H. Fei, M. Liu, S. Yazdi, J. Zhang, Q. Zhong, X. Zou, N. Zhao, H. Yu, Z. Jiang, E. Ringe, B. I. Yakobson, J. Dong, D. Chen, J. M. Tour, *ACS Nano* **2017**, *11*, 6930.
[13] H. Fei, J. Dong, Y. Feng, C. S. Allen, C. Wan, B. Volosskiy, M. Li, Z. Zhao, Y. Wang, H. Sun, P. An, W. Chen, Z. Guo, C. Lee, D. Chen, I. Shakir, M. Liu, T. Hu, Y. Li, A. I. Kirkland, X. Duan, Y. Huang, *Nat. Catal.* **2018**, *1*, 63.
[14] a) W. Chen, J. Pei, C. T. He, J. Wan, H. Ren, Y. Zhu, Y. Wang, J. Dong, S. Tian, W. C. Cheong, S. Lu, L. Zheng, X. Zheng, W. Yan, Z. Zhuang, C. Chen, Q. Peng, D. Wang, Y. Li, *Angew. Chem., Int. Ed.* **2017**, *56*, 16086; b) H. Fei, J. Dong, M. J. Arellano-Jiménez, G. Ye, N. Dong Kim, E. L. G. Samuel, Z. Peng, Z. Zhu, F. Qin, J. Bao, M. J. Yacaman, P. M. Ajayan, D. Chen, J. M. Tour, *Nat. Commun.* **2015**, *6*, 8668.
[15] a) K. Jiang, S. Siahrostami, T. Zheng, Y. Hu, S. Hwang, E. Stavitski, Y. Peng, J. Dynes, M. Gangisetty, D. Su, K. Attenkofer, H. Wang, *Energy Environ. Sci.* **2018**, *11*, 893; b) H. B. Yang, S.-F. Hung, S. Liu, K. Yuan, S. Miao, L. Zhang, X. Huang, H.-Y. Wang, W. Cai, R. Chen, J. Gao, X. Yang, W. Chen, Y. Huang, H. M. Chen, C. M. Li, T. Zhang, B. Liu, *Nat. Energy* **2018**, *3*, 140.
[16] J. K. Nørskov, T. Bligaard, A. Logadottir, J. R. Kitchin, J. G. Chen, S. Pandelov, U. Stimming, *J. Electrochem. Soc.* **2005**, *152*, J23.
[17] a) J. Greeley, T. F. Jaramillo, J. Bonde, I. Chorkendorff, J. K. Nørskov, *Nat. Mater.* **2006**, *5*, 909; b) E. Santos, P. Quaino, W. Schmickler, *Phys. Chem. Chem. Phys.* **2012**, *14*, 11224; c) N. M. Marković, P. N. Ross, *Surf. Sci. Rep.* **2002**, *45*, 117.
[18] Y. Chen, S. Ji, Y. Wang, J. Dong, W. Chen, Z. Li, R. Shen, L. Zheng, Z. Zhuang, D. Wang, Y. Li, *Angew. Chem., Int. Ed.* **2017**, *56*, 6937.
[19] a) L. Zhang, W. Liu, Y. Dou, Z. Du, M. Shao, *J. Phys. Chem. C* **2016**, *120*, 29047; b) Y. Jiao, Y. Zheng, K. Davey, S.-Z. Qiao, *Nat. Energy* **2016**, *1*, 16130.
[20] B. Hammer, J. K. Norskov, *Nature* **1995**, *376*, 238.
[21] a) Q. Gong, Y. Wang, Q. Hu, J. Zhou, R. Feng, P. N. Duchesne, P. Zhang, F. Chen, N. Han, Y. Li, C. Jin, Y. Li, S.-T. Lee, *Nat. Commun.* **2016**, *7*, 13216; b) A. Balerna, E. Bernieri, E. Burattini, A. Kuzmin, A. Lusis, J. Purans, P. Cikmach, *Nucl. Instrum. Methods Phys. Res., Sect. A* **1991**, *308*, 240.
[22] a) G. J. Colpas, M. J. Maroney, C. Bagyinka, M. Kumar, W. S. Willis, S. L. Suib, P. K. Mascharak, N. Baidya, *Inorg. Chem.* **1991**, *30*, 920; b) A. Zitolo, V. Goellner, V. Armel, M.-T. Sougrati, T. Mineva, L. Stievano, E. Fonda, F. Jaouen, *Nat. Mater.* **2015**, *14*, 937.
[23] G. Wan, P. Yu, H. Chen, J. Wen, C.-j. Sun, H. Zhou, N. Zhang, Q. Li, W. Zhao, B. Xie, T. Li, J. Shi, *Small* **2018**, *14*, 1704319.
[24] W. Chen, J. Pei, C.-T. He, J. Wan, H. Ren, Y. Wang, J. Dong, K. Wu, W.-C. Cheong, J. Mao, X. Zheng, W. Yan, Z. Zhuang, C. Chen, Q. Peng, D. Wang, Y. Li, *Adv. Mater.* **2018**, *30*, 1800396.
[25] a) P. E. Blöchl, *Phys. Rev. B* **1994**, *50*, 17953; b) G. Kresse, D. Joubert, *Phys. Rev. B* **1999**, *59*, 1758.
[26] J. P. Perdew, K. Burke, M. Ernzerhof, *Phys. Rev. Lett.* **1996**, *77*, 3865.
[27] a) G. Kresse, J. Furthmüller, *Phys. Rev. B* **1996**, *54*, 11169; b) G. Kresse, J. Furthmüller, *Comput. Mater. Sci.* **1996**, *6*, 15.
[28] G. Henkelman, A. Arnaldsson, H. Jónsson, *Comput. Mater. Sci.* **2006**, *36*, 354.
[29] W. S. Hummers, R. E. Offeman, *J. Am. Chem. Soc.* **1958**, *80*, 1339.
[30] B. Ravel, M. Newville, *J. Synchrotron Radiat.* **2005**, *12*, 537.
[31] a) J. J. Rehr, R. C. Albers, *Rev. Mod. Phys.* **2000**, *72*, 621; b) Y. Joly, *Phys. Rev. B* **2001**, *63*, 125120.